

Orbital-Dependent Dimensional Crossover of a p -Wave Feshbach Resonance

Hang Yu,^{1,*} Liao Sun,^{1,*} Shaokun Liu,¹ Shuai Peng,¹ Jiaming Li,^{1,2,3,4,†} and Le Luo^{1,2,3,4,‡}

¹*School of Physics and Astronomy, Sun Yat-Sen University, Zhuhai 519082, China*

²*Guangdong Provincial Key Laboratory of Quantum Metrology and Sensing, Sun Yat-Sen University, Zhuhai 519082, China*

³*Shenzhen Research Institute of Sun Yat-Sen University, Shenzhen 518057, China*

⁴*State Key Laboratory of Optoelectronic Materials and Technologies,
Sun Yat-Sen University, Guangzhou 510275, China*

(Dated: March 3, 2026)

We report the observation of a dimensional crossover of a narrow p -wave Feshbach resonance in an ultracold, spin-polarized ${}^6\text{Li}$ Fermi gas confined by a one-dimensional optical lattice. In the three-dimensional limit, atom loss near the resonance has a larger contribution from the $|m_l| = 1$ channel, reflecting its twofold orbital degeneracy in an isotropic system. As the lattice confinement is increased and the system approaches the quasi-two-dimensional regime, the relative contributions of the $|m_l| = 1$ and $m_l = 0$ channels evolve continuously, with an apparent suppression of the $|m_l| = 1$ feature. By quantitatively analyzing both the orbital branching ratio and confinement-induced shift of the orbital splitting, we show that this evolution arises from an orbital-dependent modification of p -wave interactions induced by reduced dimensionality. Our results establish dimensional confinement as a powerful tool for controlling orbital degrees of freedom in resonantly interacting Fermi gases, and provide new insight into how reduced dimensionality reshapes anisotropic interactions in quantum matter.

I. INTRODUCTION

Unlike s -wave scattering, p -wave interactions access collision channels with nonzero orbital angular momentum and intrinsic anisotropy [1–3]. This orbital degree of freedom enables rich few-body and many-body physics, including orbital-selective interactions and topological pairing states [4–6]. Near a magnetic Feshbach resonance, the anisotropy of p -wave scattering is strongly amplified, producing a pronounced dependence on the relative orientation between the colliding particles and the quantization axis even at ultralow energies [7–9]. Consequently, multiple scattering channels distinguished by the magnetic quantum number m_l naturally emerge.

The energy splitting between different m_l channels provides spectroscopic access to orbital-resolved scattering processes and manifests as a characteristic double-peak structure in macroscopic observables, such as atom loss induced by inelastic collisions [10–15]. By analyzing both the relative positions and amplitudes of these loss features, one can directly probe the orbital structure of a p -wave Feshbach resonance and its coupling to the scattering continuum.

A central question is how this orbital-resolved structure can be controlled in a systematic and tunable manner. Beyond magnetic-field tuning, dimensional confinement offers a powerful geometry-based knob to reshape the scattering environment and modify orbital selectivity [16–22]. In an optical lattice, confinement induces anisotropy in the relative kinetic energy, which couples directly to the orbital symmetry of p -wave scattering.

As illustrated in Fig. 1, increasing lattice depth in a one-dimensional (1D) lattice drives the system from a quasi-3D regime with substantial intersite tunneling to a quasi-2D geometry of isolated pancake-shaped sites [23], progressively suppressing relative motion along the lattice axis and redistributing the orbital contributions to scattering.

While reduced dimensionality is known to qualitatively modify p -wave scattering [24–27], establishing a direct and quantitative connection to experimentally accessible, orbital-resolved observables remains challenging. This is particularly acute for narrow p -wave resonances such as those in ${}^6\text{Li}$, where the intrinsic m_l splitting is comparable to the low-energy scales introduced by confinement. Although dimensional crossover effects have been observed in other atomic species [16, 28], a systematic and quantitative study in ${}^6\text{Li}$ —where the orbital doublet is exceptionally small—has been lacking.

Here we experimentally investigate the dimensional crossover of a narrow p -wave Feshbach resonance in a spin-polarized ${}^6\text{Li}$ Fermi gas near 159 G. Using high-resolution atom-loss spectroscopy in a 1D optical lattice, we track the evolution of the orbital doublet as the system is tuned from the quasi-3D regime to the quasi-2D limit. By analyzing both the branching ratio between the $|m_l| = 1$ and $m_l = 0$ loss channels and the orbital splitting, we decouple the effects of dimensional confinement from thermal broadening. We observe a systematic increase of the splitting between the $m_l = 0$ and $|m_l| = 1$ resonances with increasing confinement, signaling an orbital-dependent renormalization of p -wave interactions under reduced dimensionality. Our results provide a quantitative experimental characterization of how dimensional confinement reshapes the orbital-resolved structure of narrow p -wave Feshbach resonances.

* These authors contributed equally to this work.

† lijiam29@mail.sysu.edu.cn

‡ luole5@mail.sysu.edu.cn

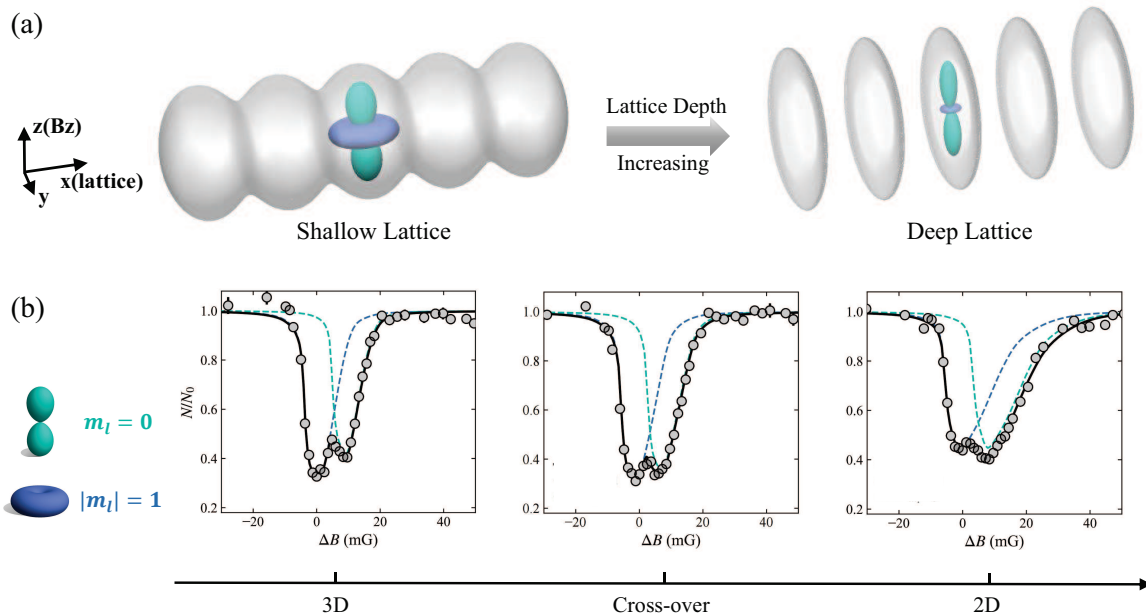


FIG. 1. Schematic of dimensional crossover and orbital anisotropy of p -wave interactions in a one-dimensional optical lattice. (a) Geometry of the lattice confinement. The magnetic field defines the quantization axis (z), while the lattice wave vector is along x . The $m_l = 0$ (teal) and $|m_l| = 1$ (blue) orbitals are indicated. Increasing lattice depth drives the system from a weakly modulated 3D geometry to an array of isolated quasi-2D pancake-shaped sites. (b) Evolution of the atom-loss spectrum across the dimensional crossover. Representative spectra are shown closed to the quasi-3D limit (left, $R = 1.94 \pm 0.25$), crossover region (middle, $R = 1.39 \pm 0.14$), and quasi-2D limit (right, $R = 1.08 \pm 0.10$). Gray circles represent the experimental data, with error bars (less than 4%) smaller than the circle size, solid black curves are total fits, and colored dashed lines indicate contributions from individual orbital branches.

II. EXPERIMENT

Following the experimental procedure described in Ref. [29], we prepare a 3D ultracold, spin-polarized Fermi gas of ${}^6\text{Li}$ atoms in the lowest hyperfine state $|1\rangle \equiv |F = 1/2, m_F = 1/2\rangle$ at a magnetic field of 320 G. The gas has a temperature of $T/T_F \approx 0.5$, where T_F is the Fermi temperature and a typical atom number of $N \approx 3 \times 10^5$.

The atoms are subsequently loaded into a 1D optical lattice oriented along the x axis. The lattice is formed by two laser beams with a wavelength of $\lambda = 1064$ nm intersecting at an angle of $2\theta = 20^\circ$. This configuration produces a lattice with a large spacing $d = \lambda/(2\sin\theta) = 3.1 \mu\text{m}$, together with an anisotropic trapping potential characterized by trap-frequency ratios $\omega_x : \omega_z : \omega_y \approx 514 : 5.8 : 1$. The lattice depth V_0 is continuously tunable up to $s = 90 E_R$, where the recoil energy is $E_R/h = 883.5$ Hz, by adjusting the laser power using an acousto-optic modulator. Further details of the experimental apparatus, cooling sequence, lattice loading procedure, and trap characterization can be found in Refs. [30, 31].

A homogeneous magnetic field B is applied along the z axis, perpendicular to the lattice direction. In this configuration, the $m_l = 0$ orbital component (teal) aligns

with the magnetic field, while the $|m_l| = 1$ components (blue) lie in the transverse x - y plane, as illustrated in Fig. 1(a). Atom-loss spectroscopy is performed near the p -wave Feshbach resonance in the $|1\rangle$ - $|1\rangle$ scattering channel, located at $B_0 \approx 159.2$ G [8].

After adiabatically loading the atoms into the lattice at a given depth V_0 , the magnetic field is ramped to a target value $B = B_0 + \Delta B$ near the resonance, where ΔB denotes the magnetic field detuning. The magnetic field is actively stabilized using a low-noise coil system with current feedback [32] and 50 Hz noise compensation [8]. This system enables a minimum field step of 1.3 mG and achieves an rms field fluctuation of 0.1 mG, providing sufficient resolution to resolve the ~ 8 mG splitting between the $m_l = 0$ and $|m_l| = 1$ resonances.

The atoms are then held for a duration t_{hold} of 350 ms, during which three-body recombination leads to atom loss. This duration is chosen to optimize the signal-to-noise ratio of the loss spectra; typically, about 20%–40% of the atoms remain at the resonance peaks, providing a high-contrast signal for resolving the m_l splitting. To accurately define t_{hold} while suppressing eddy-current-induced magnetic-field distortions, an RF-gated method is employed [29]. After the three-body reaction at the target field, the remaining atom number $N(t_{\text{hold}})$

is measured by absorption imaging after time-of-flight expansion following a rapid magnetic-field switch back to 320 G. Details of the temperature determination in this dimensional-crossover study are provided in Supplementary Material Section I. By repeating this sequence for different magnetic fields, we reconstruct the atom-loss spectrum $N(B)$; Fig. 1(b) shows three representative measured spectra, in which two distinct p -wave loss features associated with the $m_l = 0$ (right peak) and $|m_l| = 1$ (left peak) channels are clearly resolved [29]. Furthermore, by tuning the lattice depth V_0 from shallow ($s \approx 12$) to deep ($s \approx 60$), we systematically investigate how the relative contributions of the two orbital branches evolve as the system crosses over from the 3D continuum to the quasi-2D regime.

III. DATA ANALYSIS

To evaluate the atom-loss spectrum, an explicit energy-dependent description of the three-body loss is required. We therefore start from the low-energy p -wave scattering amplitude in quasi-2D geometry [25, 27],

$$f_p^{2D}(q) = \frac{4q^2}{A_p^{-1} + B_p q^2 - \frac{2}{\pi} q^2 \ln(l_x q) + i q^2}, \quad (1)$$

where q is the relative momentum and $l_x = \sqrt{\hbar/(m\omega_x)}$ is the harmonic oscillator length associated with the lattice confinement. The effective 2D scattering area A_p and effective range parameter B_p are determined by the confinement geometry according to $A_p^{-1} = (4/3\sqrt{2\pi}l_x^2)(l_x^3/V_p + k_e l_x/2 - c_1)$ and $B_p = (4/3\sqrt{2\pi})(l_x k_e - c_2)$, with $c_1 \approx 0.0655$ and $c_2 \approx 0.1464$.

The confinement-shifted resonance position B_{res} is determined by the pole condition $A_p^{-1} = 0$. Approximating the scattering volume near resonance as $V_p(B) \approx -V_{\text{bg}}\Delta B/(B - B_0)$, we obtain the confinement-induced shift [19]

$$B_{\text{res}} = B_0 - \frac{c_1 V_{\text{bg}} \Delta B}{l_x^3} + \frac{k_e V_{\text{bg}} \Delta B}{2l_x^2}. \quad (2)$$

Here we use the known ${}^6\text{Li}$ parameters $V_{\text{bg}} \approx -4.236 \times 10^4 a_0^3$, $\Delta B \approx -40.13$ G, and $k_e = 0.151 \pm 0.006 a_0^{-1}$ [8].

The confinement-induced shift in Eq. (2) arises because the lattice potential affects the open and closed channels differently. Since the open-channel scattering state has a much larger spatial extent than the tightly bound closed channel, it experiences a significant positive zero-point energy shift from the lattice confinement. This raises the energy of the open channel relative to the closed one. For the $|1\rangle - |1\rangle$ p -wave resonance, increasing the magnetic field reduces the energy gap between the two channels. Therefore, to compensate for the lattice-induced energy increase and reach the resonance condition, a higher magnetic field is required.

To incorporate inelastic three-body processes, we introduce a phenomenological imaginary contribution to

the scattering area, $A_p^{-1} \rightarrow A_p^{-1} + iA_i^{-1}$ [27]. A_i quantifies the strength of relaxation of the dimer into the deeply bound dimer states by collision with another atom [33]. This transforms Eq. (1) into an effective Breit-Wigner form,

$$f_p^{2D}(E) = \frac{2\Gamma_e(E)}{E - E_b - \Gamma_e(E)C(E) + i\Gamma_{\text{tot}}(E)/2}, \quad (3)$$

where the collision energy $E = \hbar^2 q^2/m$, the molecular binding energy $E_b = -\hbar^2/(mA_p B_p)$, and $C(E) = \frac{1}{\pi} \ln(l_x q)$. The elastic and inelastic widths are given by $\Gamma_e(E) = 2E/B_p$ and $\Gamma_{\text{in}} = 2\hbar^2/(mB_p A_i)$, respectively, yielding a total width $\Gamma_{\text{tot}}(E) = \Gamma_e(E) + \Gamma_{\text{in}}$.

The energy-dependent three-body loss coefficient is then defined as [34]

$$K_3(E) = \frac{24\pi\hbar^2}{mE} v_{\text{ad}} \sigma_p^{\text{inel}}(E), \quad (4)$$

where $\sigma_p^{\text{inel}} = \frac{2}{q}(1 - |S_p^{2D}|^2)$, $S_p^{2D} = 1 + f_p^{2D}(q)/2i$ and v_{ad} is the atom-dimer relative speed. This yields

$$K_3(E) = \frac{36\pi\hbar^3}{m^2 E} \frac{2\Gamma_e(E)\Gamma_{\text{in}}}{[E - E_b - \Gamma_e(E)C(E)]^2 + (\Gamma_{\text{tot}}/2)^2}. \quad (5)$$

For the multi-parameter fit, we treat the resonance positions of the two orbital channels as free parameters. They are defined via the resonance position B_{res} and the orbital splitting δB such that $B_{\text{res}}^1 = B_{\text{res}}$ and $B_{\text{res}}^0 = B_{\text{res}} + \delta B$. The binding energy E_b in Eq. (5) is then calculated for each channel using its respective resonance position.

Finally, the thermally averaged three-body loss coefficient $Q_3(T, B, B_{\text{res}})$ is obtained by integrating $K_3(E)$ over a Boltzmann energy distribution,

$$Q_3(T, B, B_{\text{res}}) = \frac{3}{k_B T} \int_0^\infty K_3(E) e^{-E/(k_B T)} dE. \quad (6)$$

Here the energy-dependent loss rate $K_3(E)$ implicitly depends on the magnetic field B through the detuning from B_{res} , and this dependence is suppressed in the notation for simplicity.

The measured atom-loss spectra are analyzed using a three-body recombination rate equation,

$$\frac{dN_s}{dt} = -\frac{\kappa}{3(2\pi\sigma_r^2)^2} [r_1 Q_3^1 + (1 - r_1) Q_3^0] N_s^3, \quad (7)$$

where $Q_3^0 = Q_3(T, B, B_{\text{res}}^0)$ and $Q_3^1 = Q_3(T, B, B_{\text{res}}^1)$ denote the thermally averaged three-body loss coefficients associated with the $m_l = 0$ and $|m_l| = 1$ channels, respectively. The dimensionless parameter r_1 ($0 \leq r_1 \leq 1$) characterizes the fractional contribution of the $|m_l| = 1$ channel to the total three-body loss. The geometric factor $(2\pi\sigma_r^2)^2$ originates from the mean-square atomic density per lattice site. In the radial directions, the atomic

density within each site is well approximated by a thermal Gaussian distribution with an effective width σ_r ,

$$\sigma_r^2 = \frac{k_B T}{m\omega_r^2}, \quad \omega_r = \sqrt{\omega_y \omega_z}, \quad (8)$$

where m is the atomic mass, and the mean atom number per lattice site N_s is obtained by dividing the total atom number N by the number of occupied lattice sites (27 in our experiment).

Equation (7) admits an analytical solution,

$$N_s(t) = \frac{N_s(0)}{\sqrt{1 + \frac{2\kappa t}{3(2\pi\sigma_r^2)^2} [r_1 Q_3^1 + (1-r_1)Q_3^0] N_s(0)^2}}, \quad (9)$$

where $N(0)$ is the initial atom number.

Equation (9) quantitatively reproduces both the resonance positions and the overall loss profiles across all lattice depths with a set of floating parameters B_{res} , δB , A_i , r_1 , T_{eff} , and κ . In this procedure, the effective radial width σ_r and the thermal averaging in Eq. (6) are both determined by the effective temperature T_{eff} , which is treated as a free parameter to account for the lattice-induced heating and the finite trap depth (see Supplementary Material Section II for details). Details on the interpretation of A_i and κ are provided in Supplementary Material Section III.

As demonstrated by the solid curves in Fig. 1(b), this framework provides a quantitative description of the atom-loss spectra throughout the dimensional crossover. By explicitly incorporating the confinement-modified two-body scattering amplitude while retaining the short-range three-body dynamics at a phenomenological level, the model captures the essential energy and orbital dependence of the loss process without invoking a full microscopic theory in the crossover regime.

IV. RESULTS

We define the orbital branching ratio as $R \equiv r_1/(1-r_1)$, and the extracted values are summarized in Fig. 2(a). As the lattice depth increases, R evolves systematically. In shallow lattices [left side of Fig. 1(b)], atom loss is stronger in the $|m_l| = 1$ channel, reflecting its twofold orbital degeneracy ($m_l = \pm 1$), whereas the $m_l = 0$ channel contains only a single component, so that R approaches the isotropic 3D limit $R_{3D} = 2$. With increasing confinement [middle of Fig. 1(b)], the $|m_l| = 1$ contribution is progressively suppressed and becomes comparable to that of the $m_l = 0$ branch. In the deepest lattices [right side of Fig. 1(b)], the apparent $|m_l| = 1$ feature even becomes weaker than the $m_l = 0$ peak. This apparent inversion does not indicate a reversal of the intrinsic orbital branching, but arises from the exceptionally small separation in the ${}^6\text{Li}$ p -wave Feshbach resonance, which leads to substantial spectral overlap under quasi-2D confinement. When this overlap is properly accounted for

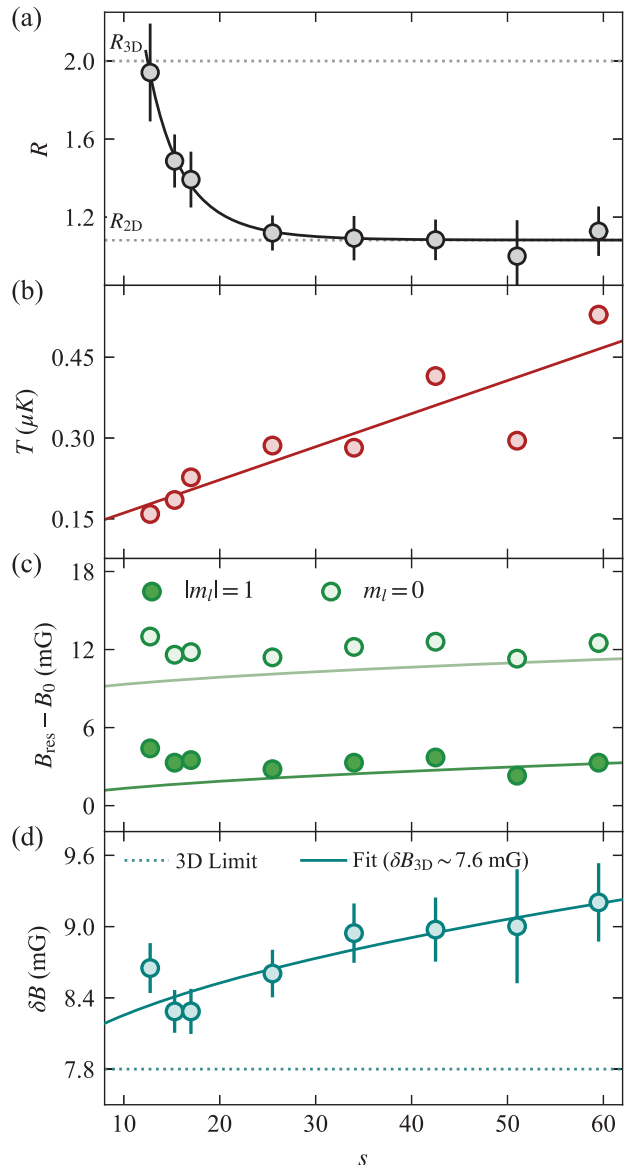


FIG. 2. Branching ratio R (a), temperature T (b), resonance positions (c), and resonance splitting δB which has a systematic error with (d) versus lattice depth s , with solid lines indicating fits or model-based calculations, as described in the text. The horizontal dotted line in (d) indicates the experimentally measured 3D limit $\delta B_{3D} = 7.8$ mG [29].

within the quasi-2D model in Eq. 9, the intrinsic branching ratio remains above unity throughout the crossover. Accordingly, R decreases monotonically and asymptotically approaches the 2D limit $R_{2D} = 1$. Physically, this trend is consistent with the confinement-induced suppression of relative motion along the lattice axis, which drives the crossover from an isotropic 3D orbital degeneracy to quasi-2D kinematic constraints.

Once the axial zero-point energy $\hbar\omega_x$ becomes larger

than the characteristic collision energy, axial relative motion is exponentially suppressed, driving a continuous crossover toward quasi-two-dimensional scattering. A quantitative interpretation of this suppression, based on the lattice-induced anisotropy of the relative kinetic energy, is provided in the Supplementary Material Section I. We therefore fit the data using the phenomenological tight-binding form

$$R(s) = R_{2D} + A_R \exp[-\gamma\sqrt{s}], \quad (10)$$

where A_R is a free amplitude parameter. The fit yields an asymptotic quasi-2D limit $R_{2D} = 1.08 \pm 0.02$ and a decay constant $\gamma = 2.01 \pm 0.27$. Remarkably, the extracted γ perfectly matches the theoretical scaling exponent of the lowest-band tunneling amplitude, $J(s) \propto \exp(-2\sqrt{s})$ [35]. This quantitative agreement confirms that the continuous evolution of the orbital branching ratio is fundamentally driven by the progressive suppression of intersite tunneling. Motivated by this behavior, we next investigate how lattice confinement modifies the resonance position B_0 and the corresponding splitting δB , providing further insight into the interplay between reduced dimensionality and anisotropic interactions.

The temperature T (see Supplementary Material Section II for details) increases gradually with lattice depth, as shown in Fig. 2(b). The absolute resonance positions B_{res} , referenced to the free-space resonance B_0 [36], are presented in Fig. 2(c), where the solid curves indicate the threshold shifts predicted by Eq. (2). Importantly, the orbital splitting δB [Fig. 2(d)] is extracted directly by fitting the double-peak lineshape of individual loss spectra. Extracting the splitting from a single spectrum effectively suppresses the influence of the slow magnetic-field drifts, allowing us to reliably resolve a systematic increase of the splitting. Fitting δB to the phenomenological form $\delta B(s) = \delta B_{3D} + A_B \sqrt{s}$ yields $\delta B_{3D} = 7.6 \pm 0.3$ mG and $A_B = 0.2 \pm 0.1$, which is in good agreement with the 3D experimental measurement of 7.8 mG [29]. This enhanced splitting indicates an orbital-dependent renormalization of p -wave interactions induced by quasi-2D confinement, beyond a simple uniform shift of the scattering threshold.

To isolate confinement effects from thermal contributions, we performed additional measurements (Fig. 3). First, by adjusting the initial depth of the 3D optical dipole trap, we achieved comparable temperatures at different lattice depths. Because of limited evaporative cooling efficiency and additional lattice-induced heating, T could be stabilized only over a narrow depth range. Figure 3(a) compares δB for two representative temperatures, $T \approx 0.21 \mu\text{K}$ and $0.29 \mu\text{K}$. For $T \approx 0.29 \mu\text{K}$, δB saturates at ~ 9 mG for $s \gtrsim 30$, showing negligible temperature dependence. For $T \approx 0.21 \mu\text{K}$, δB varies more sensitively for $15 \lesssim s \lesssim 35$, but again confirms that temperature is not the dominant factor.

Second, at fixed lattice depths $s = 17$ and 42 , the gas temperature was varied (Fig. 3(b)). In both cases, δB remained consistent within experimental uncertainty,

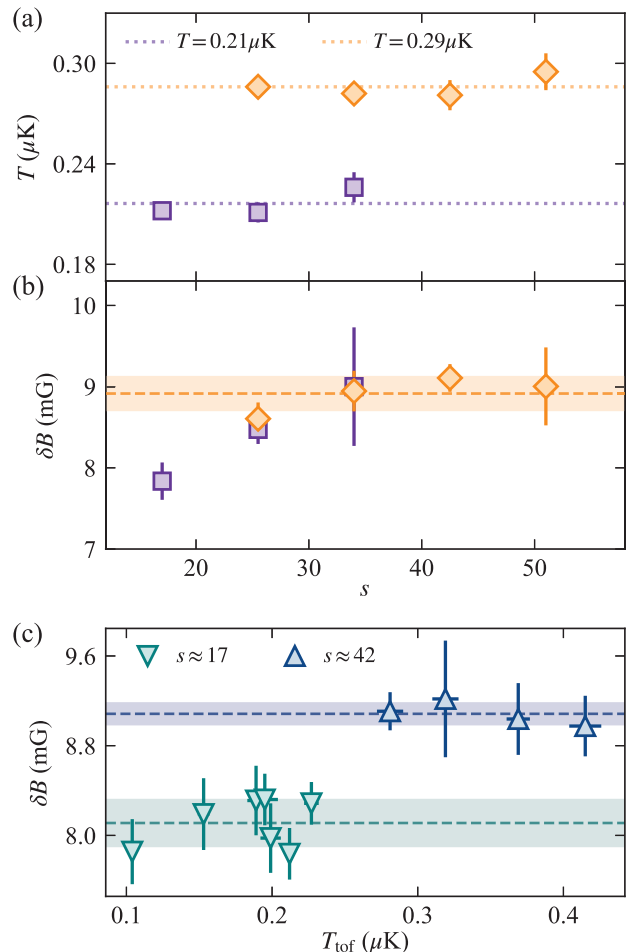


FIG. 3. Temperature dependence of the resonance splitting. (a) T versus lattice depth s . (b) Resonance splitting δB versus s , with a mean value of 8.92 mG (dashed line). (c) Splitting δB versus T_{tof} at fixed lattice depths. The dashed lines indicate mean values of 8.07 mG for $s \approx 17$ and 9.17 mG for $s \approx 42$. Error bars and shaded regions represent the standard deviation.

demonstrating that the observed enhancement of the orbital splitting is predominantly driven by lattice confinement rather than thermal effects. To further quantify the lattice-depth dependence of δB , a full coupled-channel calculation is required to incorporate both the lattice confinement and the underlying multichannel p -wave interactions.

V. CONCLUSION AND DISCUSSION

Using high-stability atom-loss spectroscopy in a one-dimensional optical lattice, we have resolved the orbital doublet of a narrow p -wave Feshbach resonance in ${}^6\text{Li}$ Fermi gas and followed its evolution across a controlled dimensional crossover from three to quasi-two dimen-

sions. The two resonance branches remain spectrally distinguishable over a wide range of lattice depths, enabling a systematic study of both their relative strengths and confinement-induced orbital splitting.

We find that the orbital branching ratio between the $|m_l| = 1$ and $m_l = 0$ channels evolves smoothly with increasing lattice depth, approaching the isotropic 3D limit at weak confinement and the expected quasi-2D limit at strong confinement. This continuous evolution demonstrates that the dimensional crossover does not induce a sharp orbital transition, but instead redistributes the loss strength between orbital channels in a controlled and geometry-dependent manner. The observed behavior is consistent with the gradual suppression of motion along the lattice axis under tight confinement.

Beyond the branching ratio, we observe a pronounced and nontrivial increase of the resonance splitting between the two orbital branches with increasing lattice depth. Through systematic temperature-controlled measurements, we explicitly disentangle thermal effects from confinement-induced shifts and show that the enhancement of the splitting is predominantly driven by lattice confinement. This enhanced relative separation indicates an orbital-dependent modification of the p -wave scattering induced by reduced dimensionality. For the exceptionally narrow p -wave resonance in ${}^6\text{Li}$, this effect is strongly amplified and becomes directly observable.

Our results establish dimensional confinement as a powerful and experimentally accessible control knob for engineering orbital-dependent interactions in quantum gases. They provide benchmarks for future microscopic theories of p -wave scattering in reduced dimensions and open opportunities for exploring anisotropic pairing, orbital-selective correlations, and topological superfluid phases in low-dimensional Fermi systems.

VI. ACKNOWLEDGEMENTS

This work is supported by NSFC under Grant No. 12174458 and No. 12574302. J. Li received support from the Fundamental Research Funds for the Central Universities, Sun Yat-sen University (24xkjc015). L. Luo received supports from Shenzhen Science and Technology Program JCYJ20220818102003006.

SUPPLEMENTARY MATERIAL

I. Kinetic energy anisotropy and branching ratio

We develop a kinetic-energy-based description that relates the orbital branching ratio to the anisotropic relative momentum distribution imposed by a one-dimensional optical lattice.

The lattice confinement modifies the long-range scattering states and induces anisotropy in the relative momentum distribution. Since the lattice length scale is much larger than the van der Waals range, we assume that short-range three-body physics remains unaffected by the lattice potential. Under this assumption, the relative weight of different p -wave resonance branches can be estimated from the angular projection of the scattering states onto the momentum distribution $n(\mathbf{k})$ [27],

$$Q_3^{m_l} \propto \int d^3\mathbf{k} n(\mathbf{k}) |Y_{1,m_l}(\hat{\mathbf{k}})|^2, \quad (11)$$

where the spherical harmonics are defined with respect to the magnetic-field axis.

Using $|Y_{1,0}|^2 \propto k_z^2/k^2$ and $|Y_{1,\pm 1}|^2 \propto (k_x^2 + k_y^2)/k^2$, the branching ratio can be written as

$$R \equiv \frac{Q_3^1}{Q_3^0} \simeq \frac{\langle k_x^2 + k_y^2 \rangle}{\langle k_z^2 \rangle} = \frac{\langle E_{\text{kin},x} \rangle + \langle E_{\text{kin},y} \rangle}{\langle E_{\text{kin},z} \rangle}. \quad (12)$$

In a shallow lattice, the momentum distribution is approximately isotropic, yielding the three-dimensional limit $R \simeq 2$. As the lattice depth increases, motion along the lattice axis becomes progressively constrained by the finite bandwidth of the lowest Bloch band, while the in-plane motion remains weakly affected. In the deep-lattice limit, the relative kinetic energy is therefore nearly isotropic within the transverse plane, leading to the quasi-two-dimensional limit $R \rightarrow 1$.

To describe this crossover quantitatively, we introduce a phenomenological model guided by the energy scales controlling axial relative motion in the lattice. In a one-dimensional optical lattice, the available axial kinetic energy is bounded by the bandwidth of the lowest Bloch band, which is set by the tunneling amplitude $J(s)$. For a sinusoidal lattice potential, $J(s)$ decreases exponentially with lattice depth as $J(s) \propto s^{3/4} \exp(-2\sqrt{s})$ [35]. This exponential suppression of motion along the lattice axis naturally suggests a smooth crossover of the branching ratio with increasing confinement.

Rather than performing a microscopic calculation of the full momentum distribution, we use this scaling behavior as a guiding principle. This motivates the phenomenological tight-binding ansatz

$$R(s) = R_{2D} + A_R \exp(-\gamma\sqrt{s}), \quad (13)$$

where R_{2D} represents the asymptotic branching ratio in the quasi-2D limit, γ characterizes the decay rate associated with the tunneling amplitude, and A_R is a free

amplitude parameter unconstrained by the isotropic 3D limit.

We note that within the confinement-induced resonance framework, the transverse motion is projected onto the lowest mode and the theory primarily renormalizes the resonance position. It does not predict the relative scattering weight of different p -wave components, so the observed evolution of the branching ratio R must be attributed to the lattice-induced anisotropy of the open-channel kinetic energy described above.

A fully microscopic description of the branching ratio in an optical lattice would require treating p -wave scattering in the basis of lattice Bloch states. In principle, this could be approached by replacing the free-space Green's function with a lattice Green's function constructed from Bloch-band dispersions, as has been explored for s -wave interactions in optical lattices [37]. Such a formulation may provide a route toward a quantitative description of the anisotropic relative kinetic energy and its impact on the orbital branching ratio, but a detailed development of this lattice-based scattering theory for p -wave interactions is beyond the scope of the present work.

II. Characterization of sample temperature

In analyzing the dimensional crossover, we employ two temperature-related quantities: the time-of-flight temperature T_{tof} and the effective temperature T_{eff} extracted from theoretical fits. Although both are expressed in temperature units, they probe distinct aspects of the system.

T_{tof} characterizes the in-plane kinetic energy and is obtained from the radial expansion of the cloud. By measuring the transverse size $\sigma_z(\tau)$ at various time-of-flight τ and fitting to the ballistic expansion relation $\sigma_z^2(\tau) = \sigma_{z0}^2 + (k_B T_{\text{tof}}/m)\tau^2$, we obtain a direct, model-independent estimate of the gas temperature. We note that the observed increase in temperature with lattice depth arises from the finite trap depth in our loading sequence, where deeper lattices naturally retain a larger fraction of high-energy atoms.

T_{eff} is the phenomenological temperature entering the thermal averaging of three-body loss coefficients in the theoretical model. It is treated as a fit parameter when analyzing the branching ratio and loss data (see Data Analysis). As shown in Fig. 4, T_{eff} remains in quantitative agreement with T_{tof} across all lattice depths, confirming that our thermometry is reliable throughout the crossover and that the observed evolution of orbital-resolved loss features is dominated by confinement rather

than temperature variations.

III. Lattice-depth dependence of the fitted loss strength

In the phenomenological fit, the product $A_i \times \kappa$ characterizes the overall strength of inelastic loss. Figure 4(b) shows that $A_i \times \kappa$ decreases monotonically with increasing lattice depth s . This trend indicates a progressive suppression of inelastic loss processes as the lattice confinement is strengthened.

Here $A_i \times \kappa$ is a fit-derived quantity and should be regarded as an effective loss strength rather than a microscopic three-body coefficient. The observed reduction of $A_i \times \kappa$ with increasing s is consistent with the experimental observation that strong lattice confinement suppresses loss, and provides a phenomenological measure of this suppression.

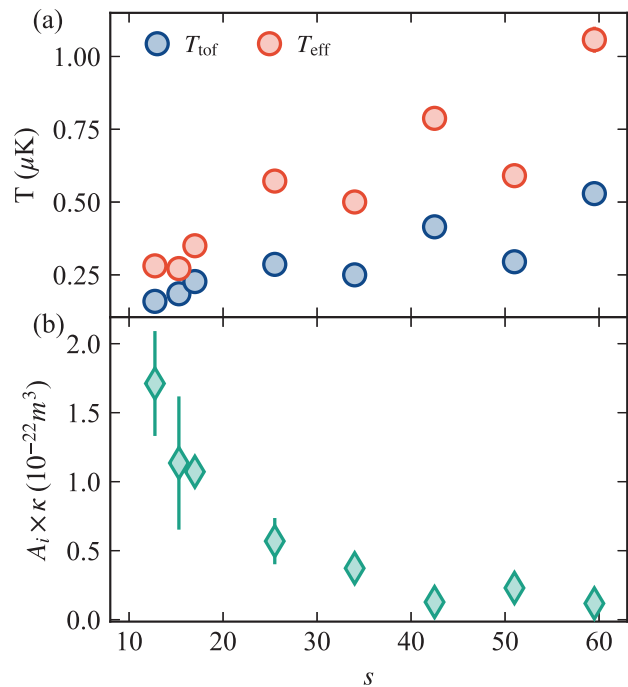


FIG. 4. (a) Comparison of the measured time-of-flight temperature T_{tof} (blue circles) and the effective fit temperature T_{eff} (red circles) as a function of lattice depth s . While there is a systematic offset, both temperatures exhibit a consistent increasing trend with lattice depth. (b) The fitted product $A_i \times \kappa$ shows a monotonic decrease with increasing lattice depth s , reflecting a reduced effective loss strength in the deep-lattice regime.

[1] C. Ticknor, C. A. Regal, D. S. Jin, and J. L. Bohn, Multiple structure of feshbach resonances in nonzero partial

waves, Phys. Rev. A **69**, 042712 (2004).

[2] T.-L. Ho and R. B. Diener, Fermion superfluids of

- nonzero orbital angular momentum near resonance, Phys. Rev. Lett. **94**, 090402 (2005).
- [3] V. Gurarie, L. Radzihovsky, and A. V. Andreev, Quantum phase transitions across a p -wave feshbach resonance, Phys. Rev. Lett **94**, 230403 (2005).
- [4] V. Gurarie and L. Radzihovsky, Resonantly paired fermionic superfluids, Ann. Phys. **322**, 2 (2007), january Special Issue 2007.
- [5] M. Sato and Y. Ando, Topological superconductors: a review, Rep. Prog. Phys. **80**, 76501 (2017).
- [6] A. Bühler, N. Lang, C. V. Kraus, G. Möller, S. D. Huber, and H.-P. Büchler, Majorana modes and p -wave superfluids for fermionic atoms in optical lattices, Nat. Commun. **5**, 4504 (2014).
- [7] C. Chin, R. Grimm, P. Julienne, and E. Tiesinga, Feshbach resonances in ultracold gases, Rev. Mod. Phys. **82**, 1225 (2010).
- [8] S. Peng, S. Peng, L. Ren, S. Liu, B. Liu, J. Li, and L. Luo, Precision measurement of spin-dependent dipolar splitting in ${}^6\text{Li}$ p -wave feshbach resonances, Phys. Rev. Lett. **135**, 133401 (2025).
- [9] K. Nagase, H. Takahashi, S. Oshima, and T. Mukaiyama, Temperature dependence of p -wave contacts in a harmonically trapped fermi gas, Phys. Rev. Lett. **136**, 013402 (2026).
- [10] H. Suno, B. D. Esry, and C. H. Greene, Recombination of three ultracold fermionic atoms, Phys. Rev. Lett. **90**, 053202 (2003).
- [11] J. H. Huckans, J. R. Williams, E. L. Hazlett, R. W. Stites, and K. M. O'Hara, Three-body recombination in a three-state fermi gas with widely tunable interactions, Phys. Rev. Lett **102**, 165302 (2009).
- [12] C. A. Regal, C. Ticknor, J. L. Bohn, and D. S. Jin, Tuning p -wave interactions in an ultracold fermi gas of atoms, Phys. Rev. Lett. **90**, 053201 (2003).
- [13] M. Gerken, B. Tran, S. Häfner, E. Tiemann, B. Zhu, and M. Weidemüller, Observation of dipolar splittings in high-resolution atom-loss spectroscopy of ${}^6\text{Li}$ p -wave feshbach resonances, Phys. Rev. A **100**, 050701 (2019).
- [14] S. Peng, T. Shu, B. Si, S. Peng, Y. Guo, Y. Han, J. Li, G. Wang, and L. Luo, Observation of a broad state-to-state spin-exchange collision near a p -wave feshbach resonance of ${}^6\text{Li}$ atoms, Phys. Rev. A **110**, L051301 (2024).
- [15] J. Zhang, E. G. M. van Kempen, T. Bourdel, L. Khaykovich, J. Cubizolles, F. Chevy, M. Teichmann, L. Tarruell, S. J. J. M. F. Kokkelmans, and C. Salomon, p -wave feshbach resonances of ultracold ${}^6\text{Li}$, Phys. Rev. A **70**, 030702 (2004).
- [16] K. Günter, T. Stöferle, H. Moritz, M. Köhl, and T. Esslinger, p -wave interactions in low-dimensional fermionic gases, Phys. Rev. Lett. **95**, 230401 (2005).
- [17] V. Venu, P. Xu, M. Mamaev, F. Corapi, T. Bilitewski, J. P. D'Incao, C. J. Fujiwara, A. M. Rey, and J. H. Thywissen, Unitary p -wave interactions between fermions in an optical lattice, Nature **613**, 262 (2023).
- [18] Y.-T. Chang, R. Senaratne, D. Cavazos-Cavazos, and R. G. Hulet, Collisional loss of one-dimensional fermions near a p -wave feshbach resonance, Phys. Rev. Lett. **125**, 263402 (2020).
- [19] M. Waseem, Z. Zhang, J. Yoshida, K. Hattori, T. Saito, and T. Mukaiyama, Creation of p -wave feshbach molecules in selected angular momentum states using an optical lattice, J. Phys. B **49**, 204001 (2016).
- [20] P. Naidon and S. Endo, Efimov physics: a review, Rep. Prog. Phys. **80**, 056001 (2017).
- [21] K. G. Jackson, C. J. Dale, J. Maki, K. G. S. Xie, B. A. Olsen, D. J. M. Ahmed-Braun, S. Zhang, and J. H. Thywissen, Emergent s -wave interactions between identical fermions in quasi-one-dimensional geometries, Phys. Rev. X **13**, 021013 (2023).
- [22] C. J. Dale, K. G. S. Xie, K. Pond Grehan, S. Zhang, J. Maki, and J. H. Thywissen, Emergent s -wave interactions in orbitally active quasi-two-dimensional fermi gases, Phys. Rev. A **110**, L051302 (2024).
- [23] K. Martiyanov, V. Makhalov, and A. Turlapov, Observation of a two-dimensional fermi gas of atoms, Phys. Rev. Lett. **105**, 030404 (2010).
- [24] L. Pricoupenko, Resonant scattering of ultracold atoms in low dimensions, Phys. Rev. Lett. **100**, 170404 (2008).
- [25] Z. Idziaszek, Analytical solutions for two atoms in a harmonic trap: p -wave interactions, Phys. Rev. A **79**, 062701 (2009).
- [26] S.-G. Peng, S. Tan, and K. Jiang, Manipulation of p -wave scattering of cold atoms in low dimensions using the magnetic field vector, Phys. Rev. Lett. **112**, 250401 (2014).
- [27] D. V. Kurlov and G. V. Shlyapnikov, Two-body relaxation of spin-polarized fermions in reduced dimensionalities near a p -wave feshbach resonance, Phys. Rev. A **95**, 032710 (2017).
- [28] Y. Guo, H. Yao, S. Ramanjanappa, S. Dhar, M. Horvath, L. Pizzino, T. Giamarchi, M. Landini, and H.-C. Nägerl, Observation of the 2d–1d crossover in strongly interacting ultracold bosons, Nat. Phys. **20**, 934 (2024).
- [29] S. Liu, Z. Xu, S. Peng, S. Peng, T. Shu, J. Li, and L. Luo, Orbital-resolved three-body recombination across a p -wave feshbach resonance in ultracold 6Li , Rep. Prog. Phys. **89**, 020502 (2026).
- [30] H. Gong, H. Liu, B. Jiao, H. Zhang, H. Yu, Q. Peng, S. Peng, T. Shu, Y. Zhu, J. Li, and L. Luo, Controllable production of degenerate fermi gases of ${}^6\text{Li}$ atoms in the crossover from two dimensions to three dimensions, Phys. Rev. A **107**, 053321 (2023).
- [31] H. Yu, H. Zhang, Q. Peng, L. Sun, B. Jiao, J. Li, and L. Luo, Shortcuts to adiabaticity for loading an ultracold fermi gas into higher orbital bands of one-dimensional optical lattice, Phys. Rev. Res. **7**, 043160 (2025).
- [32] H. Liu, S. Peng, B. Jiao, J. Li, and L. Luo, Ultra-low noise bipolar current source for ultracold atom magnetic system, Rev. Sci. Instrum. **94**, 053201 (2023).
- [33] M. Waseem, J. Yoshida, T. Saito, and T. Mukaiyama, Unitarity-limited behavior of three-body collisions in a p -wave interacting fermi gas, Phys. Rev. A **98**, 020702 (2018).
- [34] V. Ngampruetikorn, M. M. Parish, and J. Levinsen, Three-body problem in a two-dimensional fermi gas, Europhys. Lett. **102**, 13001 (2013).
- [35] W. Zwerger, Mott–hubbard transition of cold atoms in optical lattices, J. Opt. B: Quantum Semiclass. Opt **5**, S9 (2003).
- [36] Our data acquisition spanned several days, during which the absolute magnetic field experienced slow background drifts on the order of ~ 2 mG. This accounts for the scatter observed in the absolute resonance positions B_{res} . To establish a consistent reference frame across all datasets, the free-space resonance is calibrated to be $B_0 = 159.2268$ G. This value is extrapolated by anchoring our theoretical model to the resonance location measured at the maximum lattice depth, a choice motivated

by its minimal relative measurement error.

[37] G. Orso, L. P. Pitaevskii, S. Stringari, and M. Wouters,

Formation of molecules near a feshbach resonance in a 1d optical lattice, Phys. Rev. Lett. **95**, 060402 (2005).